Active surfaces for selective object segmentation in 3D

Jozsef Molnar[*1], Ervin Tasnadi[*1], Balint Kintses[1], Zoltan Farkas[1], Csaba Pal[1], Peter Horvath[1,2], Tivadar Danka[1]
{*molnar.jozsef, tasnadi.ervin, kintses.balint, farkas.zoltan, pal.csaba, horvath.peter, danka.tivadar*}*@brc.mta.hu*

[1] Synthetic and Systems Biology Unit
Biological Research Centre, Hungarian Academy of Sciences,
Szeged, Hungary

[2] Institute for Molecular Medicine Finland (FIMM)
University of Helsinki,
Helsinki, Finland

***Abstract*—Segmentation is a fundamental problem in image processing. In biomedical applications, for example cell analysis, it is important to recognize cells with certain shape characteristics. Although recent advances in microscopy and in experimental methods have made the culturing and imaging of cells in 3D environments possible, there is a great need for advanced image processing methods capable of handling such data. In this paper we present an energy minimization based method designed to segment individual objects in 3D satisfying certain size and shape properties. We introduce novel energy functionals designed to penalize shapes unfit to given priors. The three dimensional Euler elastica is also introduced as a new smoothness term, which causes the least possible interference with other terms. Solving the corresponding Euler-Lagrange equations, we demonstrate the selective segmentation capabilities of such priors.**

I. Introduction

Image segmentation is a fundamental problem in computer vision and the basis of most follow up statistical analyses in several applications. For example identification of cells in microscopy images is one of the major challenges in computational biology. Single-cell analysis of brain cells, bacteria or tumors leads to a better understanding of fundamental biological processes and to a more precise treatment of diseases. A variety of methods were proposed to segment cells in tissue sections and cell cultures, e.g. [1], [2], and several software packages utilise these results for further statistical analysis [3], [4]. Recent studies in biotechnology show that cells cultured in a 3-dimensional microenvironment mimic disease physiology more precisely than those cultured in 2-dimension [5], [6]. To study cell-cell interactions and create predictive models, different cell types are often mixed and 3-dimensional co-cultures and organoids are grown. The segmentation of such mixed 3D cell populations at the single-cell level is a great challenge, especially when their morphology shows high diversity. Although recent advances in light microscopy and assay preparation made it possible to successfully use these models for drug development and clinical applications, there is a great need for advanced segmentation methods to most precisely and cost effectively analyze these large-scale (often 10-100 TB) image data sets.

We approach the problem of segmenting single cells sharing similar morphologies using the 3D extension of the active contour framework [7], [8]. In [9], Molnar et al. introduced a family of shape descriptors to capture objects with predefined area, contour length, second moment, curvature or arbitrary combination of these. This model was able to precisely capture circular, elliptical and amoeba-like cell shapes. In this paper we present novel energies capable to segment 3D objects satisfying certain shape criteria. Our method is based on minimizing functionals designed to penalize shapes unfit to given parameters. We present a shape prior which forces objects to assume a prescribed surface/volume ratio. Using this prior it was possible to segment objects satisfying only the given parameters. This selective capability of the model is demonstrated on synthetic and fluorescent microscopy images.

The outline of the paper is the following. First, we briefly review the notations and conventions in Section II. The energy functionals used for segmentation are constructed in Section III, for which the corresponding Euler-Lagrange and level set equations are given in Section IV. The tests are carried out in Section V, while we discuss the results and future work in Section VI.

II. Notations and conventions

Surfaces will be denoted by $\mathbf{S} \subseteq \mathbb{R}^3$ or $\mathbf{S}(u,v) \in \mathbb{R}^3$ in parametrized form, where u and v are surface parameters. $\mathbf{S}_u, \mathbf{S}_v \in \mathbb{R}^3$ will denote the partial derivatives in the tangent space at $\mathbf{S}(u,v)$. Recall that $\mathbf{S}_u \times \mathbf{S}_v$ is normal to the surface. The inward pointing unit normal $\frac{\mathbf{S}_u \times \mathbf{S}_v}{|\mathbf{S}_u \times \mathbf{S}_v|}$ is denoted by $\mathbf{n}$. The sum curvature of the surface is denoted by K, while K_G is the Gaussian curvature. The integral $\int dS = \int \sqrt{|\mathbf{S}_u|^2|\mathbf{S}_v|^2 - (\mathbf{S}_u \cdot \mathbf{S}_v)^2} du dv$ gives the surface

*These authors contributed equally to this work.

area and $\int dV = -\frac{1}{3}\int \mathbf{S}\cdot(\mathbf{S}_u \times \mathbf{S}_v)dudv$ gives the volume of a surface $\mathbf{S}$, where dS and dV are the surface and volume element respectively.

To handle topological changes in the evolving surfaces, a level set representation is used. In this paper, level set functions are denoted by $\phi = \phi(t, \mathbf{x})$, where $t \in \mathbb{R}$ and $\mathbf{x} = (x_1, x_2, x_3) \in \mathbb{R}^3$ are the time and space variables respectively. According to this, ϕ_t denotes the partial derivative with respect to the time and $\nabla\phi$ denotes the spatial gradient $\nabla\phi = (\phi_{x_1}, \phi_{x_2}, \phi_{x_3})$. The Hessian matrix of ϕ is denoted by $\mathbf{H}(\phi) = (\phi_{x_i x_j})_{1\le i,j\le 3}$.

III. Functionals for selective object segmentation

In this section we present the functionals used for selective object segmentation.

A. Size priors

Our functionals responsible for the size of the object will serve two purposes. The *minimizer* functional will force the surface to shrink, while the *ratio* functional will force it to assume a prescribed volume. For minimizer, we use

$$\mathcal{M}_V(\mathbf{S}) = \int dV = -\frac{1}{3}\int \mathbf{S}\cdot(\mathbf{S}_u \times \mathbf{S}_v)dudv, \qquad (1)$$

which minimizes volume. The functional meant to force the objects towards certain volume is defined by

$$\mathcal{R}_V(\mathbf{S}) = \frac{1}{kV_0^k}\left(\int dV - V_0\right)^k, \qquad (2)$$

where V_0 is the preferred volume and $k \in \mathbb{N}$ is arbitrary. We refer to (2) as the volume prior. For even k, the functional prefers objects with volume V_0. For odd k it has an inflection at V_0, thus while it prefers zero volume, it has no effect on objects with volume V_0.

B. Shape prior

To control the shape of the objects, we have to use a functional which penalizes deviation from a given shape descriptor. For this purpose, we define a prior, which was designed to prefer shapes with given surface/volume ratio and is defined by

$$\mathcal{S}_\mathcal{A}(\mathbf{S}) = \frac{1}{2V_0^2}\left[\left(\int dS\right)^{\frac{3}{2}} - p\int dV\right]^2, \qquad (3)$$

where p is a fixed parameter and S_0 is the preferred surface. The functional penalizes the deviation from the ratio $p = \frac{surface^{\frac{3}{2}}}{volume}$. From now on, we refer to (3) as the amoeba prior.

The minimal value of the amoeba parameter is $p = 3\sqrt{4\pi} \approx 10.6$, which is achieved only by spheres. Thus by setting the amoeba parameter to this value, we can force objects towards spherical forms (Fig. 1).

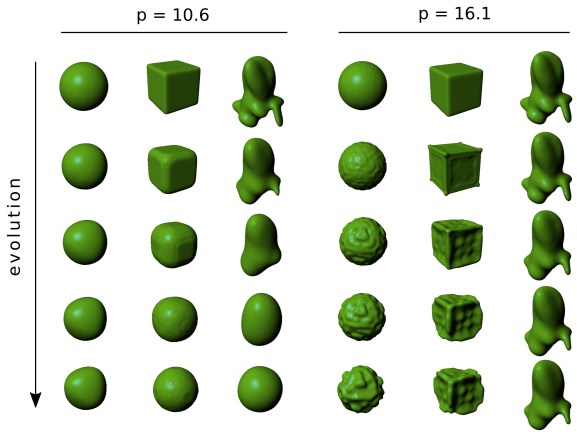

Fig. 1. Effects of the amoeba prior on various initial objects.

C. Smoothness terms

In order to avoid slow convergence or unstable behavior caused by the shape and size priors, additional functionals can be introduced to regulate the solution. In general, when higher-order derivatives are not present in the equations used for segmentation, simple smoothness terms, for example surface or volume minimizers can be used (see Section III-A). Because of interference with other terms, these will not work in our case. Instead we use the so-called *Euler elastica*, which measures the bending energy of the surface. In two dimensions, it has been applied e. g. to impainting problems [10]. For a general survey on Euler elastica, see [11]. The functional itself is defined by

$$\mathcal{E}(\mathbf{S}) = \frac{1}{2}\int K^2 dS, \qquad (4)$$

where K is the sum curvature of the surface. It is worth to note that this is a dimensionless quantity.

D. Data term

During the tests, we used the anisotropic data term (see [12])

$$\mathcal{D}(\mathbf{S}) = \int \nabla I \cdot \mathbf{n} dS, \qquad (5)$$

but in principle, a large range of data terms are feasible.

E. The composite functional for selective segmentation

In practice, the selective segmentation consists of two steps. First we find the individual objects in the image, then we turn on the shape and size priors for each object if the presegmentation had converged. Alternatively, the active surfaces can be initialized by thresholding. The two functionals we use are

$$\mathcal{L} = \alpha\mathcal{D} + \beta\mathcal{M}_V \qquad (6)$$

and

$$\mathcal{L} = \alpha\mathcal{D} + \beta\mathcal{S}_\mathcal{A} + \gamma\mathcal{R}_V + \delta\mathcal{E} \qquad (7)$$

where $\mathcal{S}_\mathcal{A}$ is the amoeba prior, $\mathcal{M}_V$ is the volume minimizing functional, $\mathcal{R}_V$ is the volume prior and $\mathcal{E}$ is the Euler elastica term used to guarantee stability and smoothness.

It is important to note that the level set equations are applied for each individual connected component of the surface, thus the speed functions for the level set evolution are only available at the points of the active surface.

IV. Euler-Lagrange formalization and level set functions

The extremal surface of a functional can be obtained by solving the corresponding Euler-Lagrange equations. In our case, these equations will have the form

$$|\mathbf{S}_u \times \mathbf{S}_v| Q\mathbf{n} = \mathbf{0}, \tag{8}$$

where Q is some scalar field, depending on the particular functional. The exact forms are specified in Section IV-A, while the methods of finding the solution is discussed in Section IV-B.

A. Differential equations for the functionals

The scalar field Q in the general Euler-Lagrange equation (8) above for the volume minimizing functional is $Q = -1$, we have $Q = -K$ for the area minimizer and $Q = \Delta I$ for the data term, where I is the image. Regarding the amoeba prior, we have

$$Q = \left[\left(\int dS\right)^{\frac{3}{2}} - p\int dV\right]\left[p - \frac{3}{2}K\left(\int dS\right)^{\frac{1}{2}}\right], \tag{9}$$

where $p = \frac{surface^{\frac{3}{2}}}{volume}$ is the given amoeba parameter describing the shape of the object. For the Euler elastica term, we obtain

$$Q = \frac{1}{2}K^3 - 2K_G K + \nabla \cdot \nabla K, \tag{10}$$

where $\nabla \cdot \nabla$ is the Laplace-Beltrami operator, which is a quantity of the tangent plane. The Euler-Lagrange equation for the Euler elastica term is calculated in Appendix A.

B. Level set formalization

To obtain the extremal surfaces minimizing the functionals, we use level set functions in combination with the gradient descent method. The Euler-Lagrange equations in Section IV-A can be translated directly to level set functions by making the substitutions

$$\mathbf{S}_u \times \mathbf{S}_v \mapsto \nabla\phi, \quad \mathbf{n} \mapsto \frac{\nabla\phi}{|\nabla\phi|}. \tag{11}$$

The curvatures of the implicit surface can be calculated with the well known formulas

$$K \mapsto -\nabla \cdot \frac{\nabla\phi}{|\nabla\phi|}, \quad K_G \mapsto |\nabla\phi|^{-4}\begin{vmatrix}\mathbf{H}(\phi) & \nabla\phi^T \\ \nabla\phi & 0\end{vmatrix}. \tag{12}$$

V. Results

This section describes the results on synthetic and fluorescent microscopy data. We present the effects of the amoeba prior on various initial shapes and the selection capabilities of the priors.

A. Synthetic tests

Fig. 1 shows the effect of the amoeba prior. In these tests, the volume and amoeba priors were used. During the evolution, the objects slowly morphed until they had reached the prescribed shape parameter. To prevent the shapes from collapsing, the volume prior (2) was used with $k = 2$.

Fig. 2 shows the selective segmentation capabilities of the model on synthesized data using the volume prior (2) in combination with the data term. Three spheroids were present in the picture, the model was parameterized to select the one in the middle and was able to segment it out based on the prescribed volume.

Fig. 3 demonstrates the selective segmentation capabilities of the amoeba prior. During these tests, the functional (7) was used. Our model was able to distinguish between spheres, cubes and ellipsoids based on their amoeba parameter p. If the shape prior is turned on, the objects are forced towards the prescribed p parameter. If this is in conflict with the objects in the image, the volume prior (2) gets pushed over its inflexion point, making the object to vanish.

B. Microscopy test

The selective segmentation results on a 3D confocal fluorescent microscopy image of cells with different shapes demonstrates that our approach can be successfully used in analyzing real microscopic images. Fig. 4 shows volume rendering of the real images containing yeast cells. Fig. 5 presents the evolution of the surface while selectively segmenting out the different cell types.

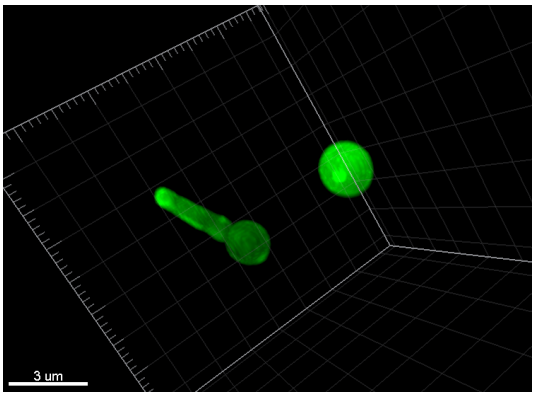

Fig. 4. Test image of two *Candida albicans* cells. The cell walls are stained using the Alexa Fluor™ 488 Concanavalin A Conjugate. The left one is in *pseudohyphae* form ($p = 22.7877$), while the one in the right side is a normal yeast form ($p = 13.4637$). The goal is to recongize the two forms by segmenting them out selectively.

VI. Conclusion and future work

In this paper, using an energy minimization framework we proposed size and shape priors for selective object segmentation. Our priors were capable of segmenting various objects based on their size and shape. We have also introduced the 3-dimensional Euler elastica as a novel smoothness term.

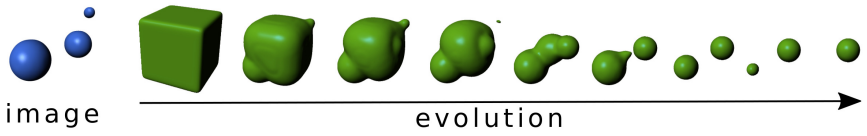

Fig. 2. Selective segmentation based on the volume prior. The V_0 in (2) was set to prefer the middle-sized sphere on the image.

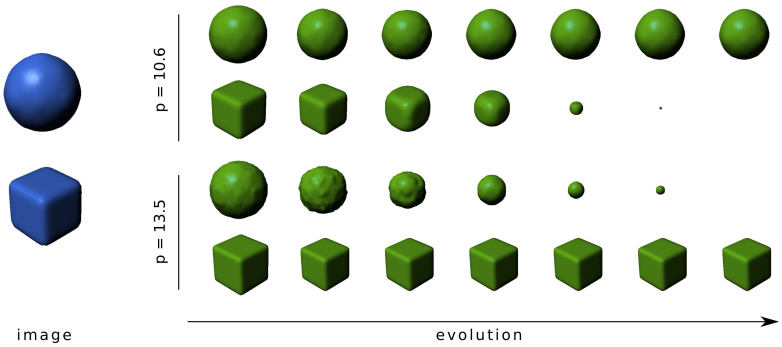

(a) A sphere and a cube

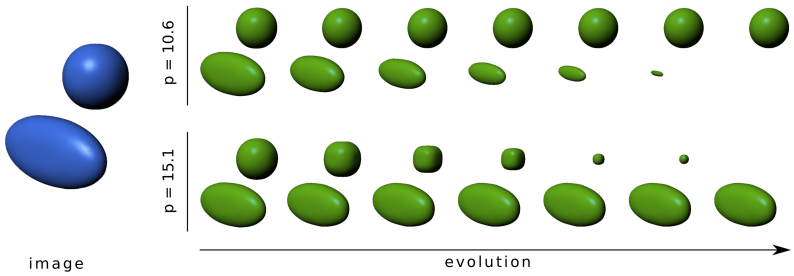

(b) A sphere and an ellipsoid

Fig. 3. Selective segmentation based on the amoeba prior. The images to be segmented are shown on the left, while the evolution of the active surfaces for distinct values of p are presented on the right. In the funcional (7), the parameters were (a) $\lambda = 135, \mu = 49, \eta = 1000, \theta = 50$ (b) $\lambda = 135, \mu = 49, \eta = 200, \theta = 50$

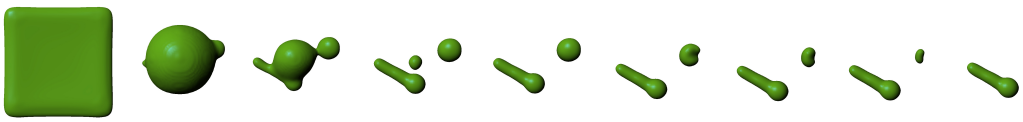

(a) Surface evolution while segmenting out the pseudohyphae form.

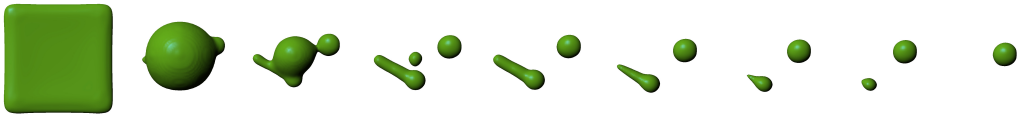

(b) Surface evolution while segmenting out the yeast cell in normal form.

Fig. 5. Selective segmentation of cells in the yeast microscopy image based on the amoeba prior. In the funcional (7), the parameters were (a) $\lambda = 0.005, \mu = 49, \eta = 1770, \theta = 50$ (b) $\lambda = 0.045, \mu = 49, \eta = 1000, \theta = 50$.

Moreover, the corresponding Euler-Lagrange equations for the minimizing surfaces are also given.

Our model had performed well on synthetic and fluorescent microscopy data. In principle, the proposed method is applicable to a wide range of problems, e.g. selective segmentation of cells based on morphological properties. As a next step we

will perform extensive tests on microscopy images to measure performance.

ACKNOWLEDGEMENTS

We acknowledge support from the Hungarian National Brain Research Program (MTA-SE-NAP B-BIOMAG: KTIA_NAP_13-2-2014-0010), from the Finnish TEKES FiDiPro Fellow Grant 40294/13, and from the European Union and the European Regional Development Funds (GINOP-2.3.2-15-2016-00001, GINOP-2.3.2-15-2016-00014, GINOP-2.3.2-15-2016-00020, GINOP-2.3.2-15-2016-00037).

APPENDIX

Here we describe the derivation of the Euler-Lagrange equation associated with a more general problem: the arbitrary function of the sum curvature with Lagrangian $L = F(K)|\mathbf{N}|$, is provided. Basic knowledge of classical differential geometry is assumed.

Additional notations: The contravariant basis vectors are denoted by $\mathbf{S}^u$, $\mathbf{S}^v$ ($\mathbf{S}^i \cdot \mathbf{S}_k = \delta^i_k$, $\delta^i_k = 1$ if $i = k$, 0 otherwise). From here on i, k, $l \in \{u, v\}$. The direct (dyadic) product of two vectors $\mathbf{u}$, $\mathbf{v}$ is defined such that $(\mathbf{uv}) \cdot \mathbf{w} = \mathbf{u}(\mathbf{v} \cdot \mathbf{w})$. Metric and inverse metric components are denoted by $g_{ik} = \mathbf{S}_i \cdot \mathbf{S}_k$ and $g^{ik} = \mathbf{S}^i \cdot \mathbf{S}^k$ respectively. The Christoffel symbols for the embedded surfaces can be defined by $\Gamma^l_{ik} = \mathbf{S}^l \cdot \mathbf{S}_{ik}$, where $\mathbf{S}_{ik}$ being the second partial derivative of the position vector. The sum and the Gaussian curvatures as formulated by Gauss are

$$K = \frac{g_{vv}(\mathbf{S}_{uu} \cdot \mathbf{n}) - 2g_{uv}(\mathbf{S}_{uv} \cdot \mathbf{n}) + g_{vv}(\mathbf{S}_{vv} \cdot \mathbf{n})}{|\mathbf{N}|^2}, \quad (13)$$

$$K_G = \frac{(\mathbf{S}_{uu} \cdot \mathbf{n})(\mathbf{S}_{vv} \cdot \mathbf{n}) - (\mathbf{S}_{uv} \cdot \mathbf{n})^2}{|\mathbf{N}|^2}, \quad (14)$$

where the denominator is the square of the normal vector $\mathbf{N} = \mathbf{S}_u \times \mathbf{S}_u$ and $|\mathbf{N}|^2$ is the determinant of the metric $|\mathbf{N}|^2 = g_{uu}g_{vv} - g^2_{uv}$. The basic differential geometry formulae used for the derivation of the Euler Lagrange equation are collected below. An arbitrary vector $\mathbf{w} \in \mathbb{R}^3$ can be decomposed at the surface points using either the covariant or the contravariant basis as

$$\begin{aligned} \mathbf{w} &= w^u \mathbf{S}_u + w^v \mathbf{S}_v + w^\perp \mathbf{n} \\ \mathbf{w} &= w_u \mathbf{S}^u + w_v \mathbf{S}^v + w^\perp \mathbf{n}, \end{aligned} \quad (15)$$

where $w^i = \mathbf{S}^i \cdot \mathbf{w}$, $w_i = \mathbf{S}_i \cdot \mathbf{w}$ and $w^\perp = \mathbf{n} \cdot \mathbf{w}$. The relations between the contravariant and covariant basis are

$$\begin{aligned} \mathbf{S}_i &= g_{iu}\mathbf{S}^u + g_{iv}\mathbf{S}^v \\ \mathbf{S}^i &= g^{iu}\mathbf{S}_u + g^{iv}\mathbf{S}_v. \end{aligned} \quad (16)$$

Note that the contravariant basis can also be expressed by the following cross products:

$$\mathbf{S}^u = \frac{1}{|\mathbf{N}|}\mathbf{S}_v \times \mathbf{n}, \ \mathbf{S}^v = \frac{1}{|\mathbf{N}|}\mathbf{n} \times \mathbf{S}_v. \quad (17)$$

The second partial derivatives of the position can be decomposed as vector is

$$\mathbf{S}_{ik} = \Gamma^u_{ik}\mathbf{S}_u + \Gamma^v_{ik}\mathbf{S}_v + (\mathbf{S}_{ik} \cdot \mathbf{n})\mathbf{n}, \quad (18)$$

where $\mathbf{I} = \mathbf{S}^u\mathbf{S}_u + \mathbf{S}^v\mathbf{S}_v + \mathbf{nn}$ being the identity tensor ($\mathbf{I} \cdot \mathbf{w} = \mathbf{w} \cdot \mathbf{I} \equiv \mathbf{w}$, $\mathbf{w} \in \mathbb{R}^3$). From (18)

$$\mathbf{S}_{ik} \cdot \mathbf{S}_l = \Gamma^u_{ik} g_{ul} + \Gamma^v_{ik} g_{vl}. \quad (19)$$

The (right) gradient of any quantity $\mathbf{X}$ restricted to the surface is defined by $\mathbf{X}\nabla \doteq \frac{\partial \mathbf{X}}{\partial u}\mathbf{S}^u + \frac{\partial \mathbf{X}}{\partial v}\mathbf{S}^v$. The divergence of a vector field $\mathbf{Y}$ is defined by $\mathbf{Y} \cdot \nabla \doteq \frac{\partial \mathbf{Y}}{\partial u} \cdot \mathbf{S}^u + \frac{\partial \mathbf{Y}}{\partial v} \cdot \mathbf{S}^v$. Simple calculation shows that the sum curvature can be expressed as the negative of the divergence of the unit normal vector:

$$K = -\mathbf{n}_u \cdot \mathbf{S}^u - \mathbf{n}_v \cdot \mathbf{S}^v = \mathbf{n} \cdot \mathbf{S}^u_u + \mathbf{n} \cdot \mathbf{S}^v_v. \quad (20)$$

The following basic identities are directly follow from the definitions:

$$\frac{\partial g_{uk}}{\partial \mathbf{S}_u} = \mathbf{S}_k \quad (21)$$

$$\frac{\partial |\mathbf{N}|}{\partial \mathbf{S}_k} = |\mathbf{N}| \mathbf{S}^k \quad (22)$$

$$\frac{\partial \mathbf{S}_{ik} \cdot \mathbf{N}}{\partial \mathbf{S}_u} = |\mathbf{N}| \left[(\mathbf{S}_{ik} \cdot \mathbf{n}) \mathbf{S}^u - \Gamma^u_{ik}\mathbf{n} \right], \quad (23)$$

e.g. for (22), formulae (17) are used. The partial derivatives of $\mathbf{n}$ and$|\mathbf{N}|$ (from (22)) are:

$$\mathbf{n}_k = -(\mathbf{n} \cdot \mathbf{S}_{uk})\mathbf{S}^u - (\mathbf{n} \cdot \mathbf{S}_{vk})\mathbf{S}^v \quad (24)$$

$$|\mathbf{N}|_k = |\mathbf{N}|(\Gamma^u_{uk} + \Gamma^v_{vk}). \quad (25)$$

In (24), decomposition (15) and $\mathbf{S}_i \cdot \mathbf{n} \equiv 0 \rightarrow \mathbf{n}_k \cdot \mathbf{S}_i = -\mathbf{n} \cdot \mathbf{S}_{ik}$, in (25) identities $|\mathbf{N}|_k = \frac{\partial |\mathbf{N}|}{\partial \mathbf{S}_u} \cdot \mathbf{S}_{uk} + \frac{\partial |\mathbf{N}|}{\partial \mathbf{S}_v} \cdot \mathbf{S}_{vk}$ are used. Starting with an equivalent expression to (13) $K = K\frac{|\mathbf{N}|}{|\mathbf{N}|}$ (to replace $\mathbf{S}_{ik} \cdot \mathbf{n}$ with $\mathbf{S}_{ik} \cdot \mathbf{N}$ in the numerator) and using formulae (21,22):

$$\begin{aligned} \frac{\partial K}{\partial \mathbf{S}_u} =& 2\frac{(\mathbf{S}_{vv} \cdot \mathbf{n})\mathbf{S}_u - (\mathbf{S}_{uv} \cdot \mathbf{n})\mathbf{S}_v}{|\mathbf{N}|^2} \\ &- \frac{g_{vv}\Gamma^u_{uu} - 2g_{uv}\Gamma^u_{uv} + g_{uu}\Gamma^u_{vv}}{|\mathbf{N}|^2}\mathbf{n} \\ &- 2K\mathbf{S}^u. \end{aligned} \quad (26)$$

Note that applying the first line of (16), the (half of the) first term of (26) can be alternatively written as

$$\begin{aligned} &\frac{g_{uu}(\mathbf{S}_{vv} \cdot \mathbf{n}) - g_{uv}(\mathbf{S}_{uv} \cdot \mathbf{n})}{|\mathbf{N}|^2}\mathbf{S}^u \\ &+ \frac{g_{uv}(\mathbf{S}_{vv} \cdot \mathbf{n}) - g_{vv}(\mathbf{S}_{uv} \cdot \mathbf{n})}{|\mathbf{N}|^2}\mathbf{S}^v. \end{aligned} \quad (27)$$

The Euler-Lagrange equation: the equation for the Lagrangian having second order derivatives can be arranged as:

$$\begin{aligned} &\frac{\partial}{\partial u}\left(-\frac{\partial L}{\partial \mathbf{S}_u} + \frac{\partial}{\partial u}\frac{\partial L}{\partial \mathbf{S}_{uu}} + \frac{1}{2}\frac{\partial}{\partial v}\frac{\partial L}{\partial \mathbf{S}_{uv}} \right) \\ &+ \frac{\partial}{\partial v}\left(-\frac{\partial L}{\partial \mathbf{S}_v} + \frac{\partial}{\partial v}\frac{\partial L}{\partial \mathbf{S}_{vv}} + \frac{1}{2}\frac{\partial}{\partial u}\frac{\partial L}{\partial \mathbf{S}_{uv}} \right). \end{aligned} \quad (28)$$

The calculations for the first three terms are as follows: a) $\frac{\partial L}{\partial \mathbf{S}_u} = |\mathbf{N}| \frac{\partial F}{\partial K} \frac{\partial K}{\partial \mathbf{S}_u}$; expanding the right side

$$\begin{aligned}\frac{\partial L}{\partial \mathbf{S}_u} &= |\mathbf{N}| \left(F - 2K \frac{dF}{dK} \right) \mathbf{S}^u \\ &+ 2\frac{dF}{dK} \frac{(\mathbf{S}_{vv} \cdot \mathbf{n}) \mathbf{S}_u - (\mathbf{S}_{uv} \cdot \mathbf{n}) \mathbf{S}_v}{|\mathbf{N}|} \\ &- \frac{dF}{dK} \frac{g_{vv}\Gamma^u_{uu} - 2g_{uv}\Gamma^u_{uv} + g_{uu}\Gamma^u_{vv}}{|\mathbf{N}|} \mathbf{n},\end{aligned} \tag{29}$$

where (26) is used; b) $\frac{\partial}{\partial u} \frac{\partial L}{\partial \mathbf{S}_{uu}} + \frac{1}{2} \frac{\partial}{\partial u} \frac{\partial L}{\partial \mathbf{S}_{uu}} = \mathbf{S}_v \cdot \frac{\partial}{\partial u} \left(\frac{dF}{dK} \frac{\mathbf{S}_v}{|\mathbf{N}|} \mathbf{n} \right) - \mathbf{S}_u \cdot \frac{\partial}{\partial v} \left(\frac{dF}{dK} \frac{\mathbf{S}_v}{|\mathbf{N}|} \mathbf{n} \right)$, using $\frac{\partial L}{\partial \mathbf{S}_{uu}} = \frac{dF}{dK} \frac{g_{vv}}{|\mathbf{N}|} \mathbf{n}$, $\frac{1}{2} \frac{\partial L}{\partial \mathbf{S}_{uv}} = -\frac{dF}{dK} \frac{g_{uv}}{|\mathbf{N}|} \mathbf{n}$, and expanding the right side

$$\begin{aligned}&\frac{\partial}{\partial u} \frac{\partial L}{\partial \mathbf{S}_{uu}} + \frac{1}{2} \frac{\partial}{\partial u} \frac{\partial L}{\partial \mathbf{S}_{uu}} \\ &= \frac{d^2F}{dK^2} \left(g_{vv} \frac{\partial K}{\partial u} - g_{uv} \frac{\partial K}{\partial v} \right) \frac{\mathbf{n}}{|\mathbf{N}|} \\ &+ \frac{dF}{dK} \frac{2g_{uv}\Gamma^u_{uv} - g_{uu}\Gamma^u_{vv} - g_{vv}\Gamma^u_{uu}}{|\mathbf{N}|} \mathbf{n} \\ &+ \frac{dF}{dK} \frac{-g_{vv} (\mathbf{S}_{uu} \cdot \mathbf{n}) + g_{uv} (\mathbf{S}_{uv} \cdot \mathbf{n})}{|\mathbf{N}|} \mathbf{S}^u \\ &+ \frac{dF}{dK} \frac{-g_{vv} (\mathbf{S}_{uv} \cdot \mathbf{n}) + g_{uv} (\mathbf{S}_{vv} \cdot \mathbf{n})}{|\mathbf{N}|} \mathbf{S}^v,\end{aligned} \tag{30}$$

where the second term is the sum given by the derivatives of the covariant basis vectors $\mathbf{S}_i$ (using (19)) and the denominator $|\mathbf{N}|$ (using (25)), whilst the third an fourth terms come from the derivatives of the unit normal vector $\mathbf{n}$ (using (24)). Adding (29,30) and using (27), the following terms remain:

$$\begin{aligned}&\frac{\partial}{\partial u} \frac{\partial L}{\partial \mathbf{S}_{uu}} + \frac{1}{2} \frac{\partial}{\partial v} \frac{\partial L}{\partial \mathbf{S}_{uv}} - \frac{\partial L}{\partial \mathbf{S}_u} \\ &= \frac{d^2F}{dK^2} \left(g_{vv} \frac{\partial K}{\partial u} - g_{uv} \frac{\partial K}{\partial v} \right) \frac{\mathbf{n}}{|\mathbf{N}|} \\ &+ \frac{dF}{dK} \frac{(\mathbf{S}_{uv} \cdot \mathbf{n}) \mathbf{S}_v - (\mathbf{S}_{vv} \cdot \mathbf{n}) \mathbf{S}_u}{|\mathbf{N}|} \\ &+ |\mathbf{N}| \left(K \frac{dF}{dK} - F \right) \mathbf{S}^u.\end{aligned} \tag{31}$$

Applying same steps for the second three terms of (28) the result is identical to (31) with the indices u, v swapped. Summing up the terms in the normal direction, the Euler-Lagrange equation (28) takes the form

$$\begin{aligned}&|\mathbf{N}| \left(K \frac{dF}{dK} - F \right) (\mathbf{S}^u_u \cdot \mathbf{n} + \mathbf{S}^v_v \cdot \mathbf{n}) \\ &+ 2\frac{dF}{dK} \frac{(\mathbf{S}_{uv} \cdot \mathbf{n})^2 - (\mathbf{S}_{uu} \cdot \mathbf{n}) (\mathbf{S}_{vv} \cdot \mathbf{n})}{|\mathbf{N}|} \\ &+ \frac{d^3F}{dK^3} \left[\frac{g_{vv}}{|\mathbf{N}|} \left(\frac{\partial K}{\partial u} \right)^2 - 2\frac{g_{vv}}{|\mathbf{N}|} \frac{\partial K}{\partial u} \frac{\partial K}{\partial v} + \frac{g_{uu}}{|\mathbf{N}|} \left(\frac{\partial K}{\partial v} \right)^2 \right] \\ &+ \frac{d^2F}{dK^2} \left[\frac{g_{vv}}{|\mathbf{N}|} \frac{\partial^2 K}{\partial u^2} - 2\frac{g_{vv}}{|\mathbf{N}|} \frac{\partial^2 K}{\partial u \partial v} + \frac{g_{uu}}{|\mathbf{N}|} \frac{\partial^2 K}{\partial v^2} \right] \\ &+ \frac{d^2F}{dK^2} \frac{\partial K}{\partial u} \left[-\frac{g_{vv}}{|\mathbf{N}|} \Gamma^u_{uu} + 2\frac{g_{vv}}{|\mathbf{N}|} \Gamma^u_{uv} - \frac{g_{uu}}{|\mathbf{N}|} \Gamma^u_{vv} \right] \\ &+ \frac{d^2F}{dK^2} \frac{\partial K}{\partial v} \left[-\frac{g_{vv}}{|\mathbf{N}|} \Gamma^v_{uu} + 2\frac{g_{vv}}{|\mathbf{N}|} \Gamma^v_{uv} - \frac{g_{uu}}{|\mathbf{N}|} \Gamma^v_{vv} \right].\end{aligned} \tag{32}$$

Similar calculation shows that the components in the tangent plane are all zero. In (32) the first term includes the sum curvature (20), the second term the Gaussian curvature (14). Simple calculation shows that the sum of the last four lines is the ($|\mathbf{N}|$ times the) divergence of the gradient i.e. the Laplace-Beltrami of $\frac{dF}{dK}$: $\frac{\partial}{\partial u} \left[\left(\frac{\partial}{\partial u} \frac{dF}{dK} \right) \mathbf{S}^u + \left(\frac{\partial}{\partial v} \frac{dF}{dK} \right) \mathbf{S}^v \right] \cdot \mathbf{S}^u + \frac{\partial}{\partial v} \left[\left(\frac{\partial}{\partial u} \frac{dF}{dK} \right) \mathbf{S}^u + \left(\frac{\partial}{\partial v} \frac{dF}{dK} \right) \mathbf{S}^v \right] \cdot \mathbf{S}^v$ (the relation between the metric and inverse metric $\left[g^{ik} \right] = \left[g_{ik} \right]^{-1}$ is used). Finally the Euler-Lagrange equation associated with the Lagrangian $L = F(K) |\mathbf{N}|$ can be written as

$$|\mathbf{N}| \left[\left(K \frac{dF}{dK} - F \right) K - 2\frac{dF}{dK} K_G + \nabla \cdot \nabla \frac{dF}{dK} \right] \mathbf{n} = \mathbf{0}, \tag{33}$$

where $\nabla \cdot \nabla$ is a usual notation for the Laplace-Beltrami operator. An alternative formula to (33) can be written as $|\mathbf{N}| \left[\left(K \frac{dF}{dK} - F \right) K - 2\frac{dF}{dK} K_G + \left(\frac{dF}{dK} \nabla \nabla \right) \cdot \cdot \mathbf{I}^{-1} \right] \mathbf{n} = \mathbf{0}$, where $\mathbf{I}$ stands for the first fundamental form i.e. the metric tensor with components g_{ik} and "$\cdot\cdot$" is the double scalar product operator (the result is the sum of the products of the corresponding components of the tensors involved in the operation). Using similar steps, one can deduce Euler-Lagrange equation for the arbitrary function of the Gaussian curvature, that turns to be

$$|\mathbf{N}| \left[2K \left(F - \frac{dF}{dK_G} \right) + K_G \left(\frac{dF}{dK_G} \nabla \nabla \right) \cdot \cdot \mathbf{II}^{-1} \right] \mathbf{n} = \mathbf{0}, \tag{34}$$

where $\mathbf{II}$ stands for the "second fundamental form" with components $\mathbf{S}_{ik} \cdot \mathbf{n}$.

REFERENCES

[1] P. Bamford and B. Lovell., "Unsupervised Cell Nucleus Segmentation with Active Contours." *Signal Processing*, vol. 71, no. 2, 1998.

[2] C. Molnar, I. H. Jermyn, Z. Kato, P. O. V. Rahkama, P. Mikkonen, V. Pietiäinen, and P. Horvath., "Accurate Morphology Preserving Segmentation of Overlapping Cells based on Active Contours." *Scientific Reports*, vol. 6, 2016.

[3] D. Dao, A. N. Fraser, J. Hung, V. Ljosa, S. Singh, and A. E. Carpenter., "CellProfiler Analyst: Interactive Data Exploration, Analysis, and Classification of Large Biological Image Sets." *Bioinformatics*, vol. 32, no. 20, 2016.

[4] F. Piccinini, T. Balassa, A. Szkalisity, C. Molnar, L. Paavolainen, K. Kujala, K. Buzas, M. Sarazova, V. Pietiainen, U. Kutay, K. Smith, and P. Horvath, "Advanced Cell Classifier: User-Friendly Machine-Learning-Based Software for Discovering Phenotypes in High-Content Imaging Data," *Cell Systems*, vol. 4, no. 6, pp. 651–655, 2017.

[5] P. Horvath, N. Aulner, M. Bickle, A. M. Davies, E. D. Nery, D. Ebner, M. C. Montoya, P. Östling, V. Pietiäinen, L. S. Price, S. L. Shorte, G. Turcatti, C. von Schantz, and N. O. Carragher., "Screening Out Irrelevant Cell-Based Models of Disease." *Nature Reviews Drug Discovery*, vol. 15, pp. 751–769, 2016.

[6] D. Wessels, D. F. Lusche, E. Voss, S. Kuhl, E. C. Buchele, M. R. Klemme, K. B. Russell, J. Ambrose, B. A. Soll, A. Bossler, M. Milhem, C. Goldman, and D. Soll., "MelanomaCcells Undergo Aggressive Coalescence in a 3D Matrigel Model that is Repressed by anti-CD44." *PLoS One*, vol. 12, no. 3.

[7] A. W. M. Kass and D. Terzopoulos., "Snakes: Active Contour Models," *International Journal of Computer Vision*, vol. 1, no. 4, pp. 321–331, 1988.

[8] D. Zhang and G. Lu, "Review of shape representation and description techniques," *Pattern Recognition*, vol. 37, no. 1, pp. 1 – 19, 2004.

[9] J. Molnar, I. A. Szucs, C. Molnar, and P. Horvath., "Active Contours for Selective Object Segmentation." in *WACV*. IEEE Computer Society, 2016, pp. 1–9.

[10] T. F. Chan, S. H. Kang, and J. Shen., "Euler's Elastica and Curvature-Based Inpainting." *SIAM Journal on Applied Mathematics*, vol. 63, pp. 564–592, 2002.

[11] D. Mumford, "Elastica and Computer Vision." in *Algebraic Geometry and its Applications: Collections of Papers from Shreeram S. Abhyankar's 60th Birthday Conference"*, C. L. Bajaj, Ed. New York, NY: Springer New York, 1994, pp. 491–506.

[12] R. Kimmel and A. Bruckstein, "Regularized Laplacian Zero Crossings as Optimal Edge Integrators." *International Journal of Computer Vision*, vol. 53, no. 3, pp. 225–243, 2003.